ATMOSPHERIC ENVIRONMENT: X 24 (2024) 100303

Contents lists available at ScienceDirect

Atmospheric Environment: X

journal homepage: www.journals.elsevier.com/atmospheric-environment-x

Comparison of global air pollution impacts across horizontal resolutions

Thanapat Jansakoo [a,*], Ryouichi Watanabe [c], Akio Uetani [a], Satoshi Sekizawa [a], Shinichiro Fujimori [a,d,e,**], Tomoko Hasegawa [a,b], Ken Oshiro [a]

[a] Department of Environmental Engineering, Kyoto University, C1-3 361, Kyotodaigaku Katsura, Nishikyoku, Kyoto city, Japan
[b] Department of Civil and Environmental Engineering, College of Science and Engineering, Ritsumeikan University, Kyoto, Japan
[c] Japan Weather Association, Tokyo, Japan
[d] Social Systems Division, National Institute for Environmental Studies (NIES), 16-2 Onogawa, Tsukuba, Ibaraki, 305-8506, Japan
[e] International Institute for Applied Systems Analysis (IIASA), Schlossplatz 1, A-2361, Laxenburg, Austria

ARTICLE INFO

Keywords:
Air pollution
Atmospheric chemistry transport model
Climate change
GEOS-Chem
Horizontal resolution
O_3
$PM_{2.5}$

ABSTRACT

The impact of ambient air pollution on human health, particularly fine particulate matter ($PM_{2.5}$) and tropospheric ozone (O_3), is a critical global concern. Atmospheric chemical transport models (CTMs) are widely used to predict air pollutant concentrations and assess associated health risks. However, there is a need to better understand how the horizontal resolution of these models influences their accuracy, especially in future assessments. In this study, we compared the performance of global low-resolution CTMs with high-resolution nested simulations for estimating O_3 and $PM_{2.5}$ concentrations. The models were validated against observational data to determine their accuracy across different spatial scales and to evaluate their suitability for future scenario assessments. Our findings demonstrate that while the nested-grid simulations improved the reproducibility of regional observations, especially in areas with complex topography or localized emissions, the overall global-scale performance of the model did not significantly benefit from higher resolution. Additionally, the differences in global health and agricultural impacts between low- and high-resolution simulations were minor and within the range of uncertainty typically associated with emission inventories and CTMs. However, for specific regional studies or policy applications, higher resolution may offer improved accuracy. Ultimately, the current low-spatial-resolution model provides sufficient accuracy for many global-scale applications, but the choice of resolution should be carefully considered depending on the specific objectives of the study especially in future scenario.

1. Introduction

Climate change is one of the most urgent and complex challenges facing modern society, with profound implications for ecosystems, economies, and human health. In addition to its global effects, climate change interacts with local air quality through a range of intricate and multifaceted processes. For example, climate change contributes to increased frequency and intensity of wildfires, leading to elevated emissions of fine particulate matter ($PM_{2.5}$) while higher temperatures from climate change can increase the formation of ground-level ozone (O_3) (Fiore et al., 2015; Jacob and Winner, 2009; Schneidemesser et al., 2015). These pollutants has detrimental consequences on human health and agricultural production (Agrawal, 2005; Ashmore, 1991; Brunekreef and Holgate, 2002).

To combat climate change, reducing greenhouse gas emissions, particularly carbon dioxide (CO_2), is a critical priority as outlined by the Kyoto Protocol (Iwata and Okada, 2014; Occhipinti and Verona, 2020). While climate change mitigation policies, such as phasing out fossil fuels, primarily aim to reduce greenhouse gas (GHG) emissions, they often have the co-benefit of improving air quality. The transition away from fossil fuels reduces the release of air pollutants, such as sulfur dioxide (SO_2), nitrogen oxides (NOx), and particulate matter (PM), which are major contributors to air pollution (Jiang et al., 2013; Nemet et al., 2010; Thurston and Bell, 2021; Vandyck et al., 2018; West et al., 2013). This benefit can lead to significant improvements in public health by lowering the incidence of respiratory and cardiovascular diseases linked to poor air quality. Thus, climate policies not only address long-term climate goals but also deliver immediate health and environmental

* Corresponding author.
** Corresponding author. Department of Environmental Engineering, Kyoto University, C1-3 361, Kyotodaigaku Katsura, Nishikyoku, Kyoto city, Japan.
E-mail addresses: jansakoo.thanapat.2a@kyoto-u.ac.jp (T. Jansakoo), fujimori.shinichiro.8a@kyoto-u.ac.jp (S. Fujimori).

https://doi.org/10.1016/j.aeaoa.2024.100303
Received 3 June 2024; Received in revised form 1 October 2024; Accepted 24 October 2024
Available online 26 October 2024

gains at the local level.

Recently, chemical transport models (CTMs) and source receptor models have been used to convert the emissions of air pollutants into atmospheric concentrations of the air pollutants (Askariyeh et al., 2020). The outcome form the CTM model can be used to assess the impacts of air pollutants such as $PM_{2.5}$ and tropospheric O_3, which are linked to significant human health risks and agricultural losses (Anenberg et al., 2010; Chuwah et al., 2015; Cissé et al., 2022; Cohen et al., 2017; Xiong et al., 2022). CTMs are particularly useful for capturing complex chemical-transport interactions, although they require substantial computing power. In contrast, source-receptor models are less computationally intensive but may not account for nonlinear interactions as effectively. Given these constraints, global CTM simulations often use coarse horizontal resolutions, which may limit the accuracy of the outcomes. One approach to improving this is to use nested-grid simulations, which focus on a specific region with finer spatial resolution (Chen et al., 2009; Protonotariou et al., 2010; Zhang et al., 2011). However, the impact of horizontal resolution on simulation accuracy remains unclear, making it important to evaluate whether finer resolutions provide significant advantages. The primary objective of this study is to evaluate the accuracy of nested-grid simulations by comparing them with global-grid models to assess whether the increased resolution significantly enhances predictive accuracy. Additionally, we apply our modeling framework to future scenarios, focusing on the co-emission of greenhouse gases (GHGs) and air pollutants. Given the uncertainty surrounding the necessity of nested simulations, this study examines whether higher resolution is essential for drawing robust conclusions in future research. It is important to note that our study does not directly address the climate change penalty on air quality.

Our hypothesis is that while nested-grid simulations have the potential to provide more detailed air quality predictions, their impact on the overall accuracy of PM2.5 and O_3 predictions and their broader social and environmental implications remains uncertain. Although the nested-grid approach offers finer spatial resolution and is expected to capture localized variations more effectively, no comprehensive study has yet evaluated its accuracy compared to global low-resolution models in the context of future air quality assessments.

In this study, we assess the effectiveness of nested-grid ($0.5^\circ \times 0.625^\circ$) simulations compared to global-grid ($4.0^\circ \times 5.0^\circ$) simulations in predicting air pollutant concentrations using the GEOS-Chem model. This model is driven by meteorological inputs provided by the NASA Global Modeling and Assimilation Office, ensuring accurate representation of atmospheric conditions. For emissions flux data, we utilize gridded emissions from Integrated Assessment Models (IAMs), specifically The Asia-Pacific Integrated Model (AIM-Hub). This approach allows for a comprehensive evaluation of the model's performance across different spatial resolutions, providing insights into the strengths and limitations of each configuration in predicting air quality under various emission scenarios. To assess the accuracy of the GEOS-Chem model, we compare simulation outcomes for the year 2015 with observational data from ground monitoring stations. This study extends the evaluation to future scenarios, exploring whether resolution-induced discrepancies in impact assessments become more pronounced over time. By focusing on the effects of different resolutions on both present and projected air quality, particularly in the context of evolving climate policies, we aim to determine if present-day discrepancies persist or intensify in future conditions. Notably, this study does not account for future climate feedback from changes in GHG emissions, as our primary focus is on the impact of climate change policies on co-emissions of GHGs.

In summary, this study evaluates the influence of horizontal resolution on global simulation outcomes to determine the most effective approach for assessing air pollution in the context of climate change mitigation. If higher-resolution models are found to be non-essential, environmental assessments could be conducted accurately and more efficiently, enabling quicker evaluations. This would particularly benefit studies examining air pollution impacts within IAMs, allowing for rapid assessment of air quality issues related to new climate policies without the need for intensive computing, thus providing results almost immediately.

2. Methodology

We used the GEOS-Chem model to predict the ground surface concentrations of $PM_{2.5}$ and O_3 using an air pollution emission inventory and meteorological data as inputs in the simulations with ($0.5^\circ \times 0.625^\circ$) and without ($4^\circ \times 5^\circ$) nested grids (Fig. 1). We implemented several future emissions scenarios derived from AIM so that the validity of the nested-grid simulation could be tested under multiple plausible future scenarios. We conducted two types of assessment. First, we compared the simulated $PM_{2.5}$ and O_3 concentrations with monitoring data to confirm the validity of the simulation results at both resolutions. Second, crop production losses caused by O_3 and the mortality changes due to $PM_{2.5}$ exposure were used to evaluate how the resolution would change the implications for the human social system.

2.1. Model description

2.1.1. GEOS-chem

We used a chemical transport model (CTM) to simulate the distribution of $PM_{2.5}$ and ozone in the atmosphere. For this, we relied on GEOS-Chem, a global 3-D model of atmospheric composition that helps track how chemicals move and change in the atmosphere. We used version 12.9.3 of GEOS-Chem, driven by NASA Global Modeling and Assimilation Office's MERRA2 reanalysis weather data (Bey et al., 2001; v12-09, http://www.geos-chem.org). This weather data can be less detailed when using a lower-resolution grid. For example, when we ran the simulation at a global scale with a coarser resolution of $4.0^\circ \times 5.0^\circ$, the original high-resolution MERRA2 weather data (which has a grid resolution of $0.5^\circ \times 0.625^\circ$) was aggregated to match the coarser grid. This aggregation reduces the level of detail in the meteorological inputs, which can affect the precision of the simulated atmospheric processes at this scale.

In our study, we ran simulations at two different scales: a global scale with a global grid resolution of $4.0^\circ \times 5.0^\circ$ (Fig. 2: gray) and a regional scale with a finer grid resolution of $0.5^\circ \times 0.625^\circ$, known as a nested simulation (Fig. 2: red). The choice of the nested simulation was influenced by the emission data we used, which came from the AIM-Hub model, limiting us to a 0.5-degree resolution. We configured the GEOS-Chem model to include 72 vertical layers, which allowed us to capture the atmosphere's chemical composition at different heights. Before starting the main simulation, we ran a two-month spin-up period. This preliminary phase helped the model balance and stabilized atmospheric and chemical processes, ensuring that the results from the main study period would be more accurate and realistic. Regarding the transboundary transport, the GEOS-Chem model uses a one-way coupling configuration for nested-grid simulations, where the global model supplies boundary conditions to the nested grids without feedback from nested back to the global domain.

GEOS-Chem included a detailed chemical mechanism involving O_x–NO_x–hydrocarbon–aerosol–bromine (Mao et al., 2013; Parrella et al., 2012). In the GEOS-Chem model, $PM_{2.5}$ is composed of natural mineral dust, sea salt, primary BC aerosols, primary organic aerosols, secondary inorganic aerosols (sulfate, nitrate, and ammonium), and secondary organic aerosols. In addition, ISORROPIA II was used to simulate the thermodynamics of secondary inorganic aerosols (Fountoukis and Nenes, 2007; Pye et al., 2010).

2.1.2. AIM-Hub

The Asia-Pacific Integrated Model (AIM-Hub) modeling framework allows the quantification of future scenarios. This comprehensive model framework, as presented by Fujimori et al. (2018), facilitated the evaluation of critical sectors, including energy, land use, agriculture, GHG

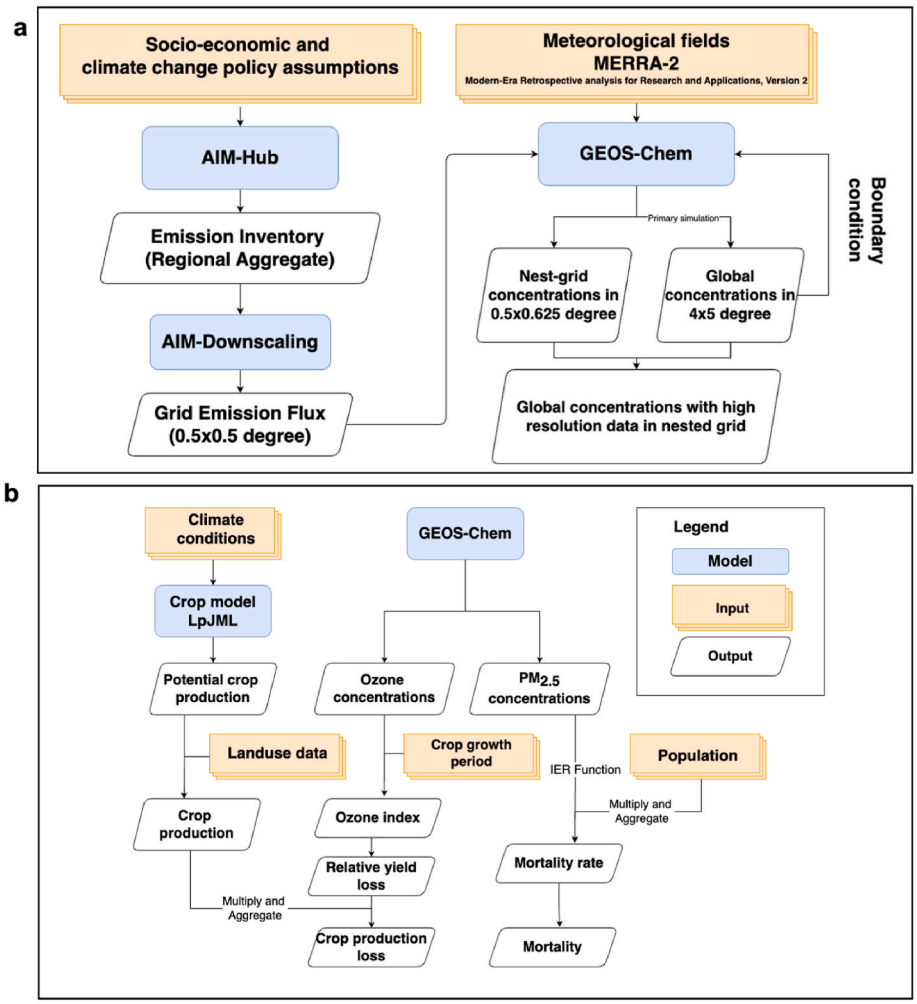

Fig. 1. The framework of GEOS-Chem simulations (top) and the impact assessment (bottom).

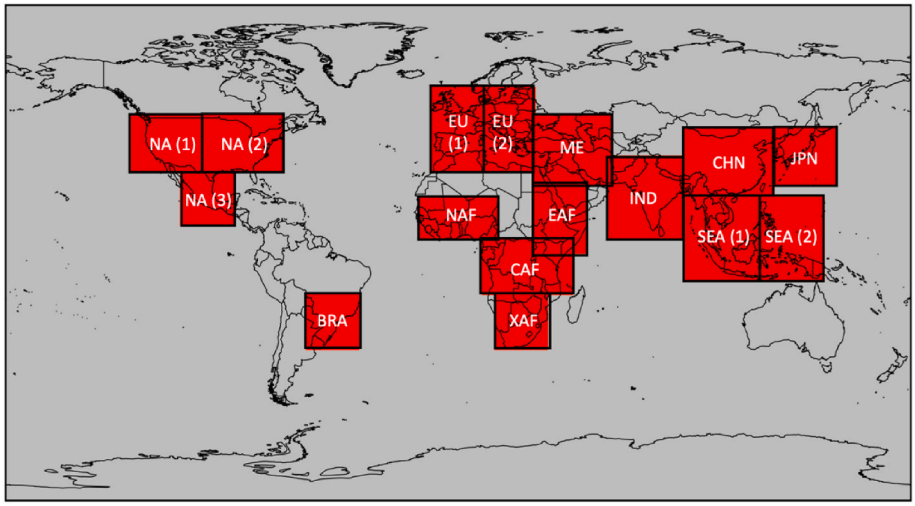

Fig. 2. GEOS-Chem nested-grid domain (0.5° × 0.625°: red) for the target area. BRA = Brazil; NA = North America; CHN = China; EU=Europe; IND = India; JPN = Japan; ME = Middle East; SEA = Southeast Asia; NAF = North Africa; EAF = East Africa; CAF = Central Africa; XAF = South Africa. (For interpretation of the references to colour in this figure legend, the reader is referred to the Web version of this article.)

emissions, and air pollutant emissions. The framework adopts the Shared Socioeconomic Pathways (SSPs) for scenario development, focusing on population and economic projections. For this study, we applied the SSP2 scenario, known as the "middle of the road" scenario, as outlined by O'Neill et al. (2017). Details regarding the model structure and mathematical formulation are extensively documented in Fujimori

et al. (2012).

The model assumes that production sectors aim to maximize profits using multi-nested constant elasticity substitution (CES) functions, taking into account input prices. Emissions from land-use changes are computed by considering the variations in forest area relative to the previous year, adjusted by carbon stock densities specific to global agroecological zones. Non-energy-related emissions, excluding land-use changes, are assumed to correlate directly with activity levels, such as production output (Fujimori et al., 2022). To illustrate the variations in emissions associated with land-use changes, we have included a figure in the supplementary material (Fig. A1), showing the trends in global land-use-related CO_2 emissions. This figure captures the regional dynamics and temporal changes in emissions from land use, offering a clearer picture of how these emissions evolve from 2015 to 2100 under the AIM-Hub framework.

The model was calibration across various sectors with the Global Trade Analysis Project (GTAP) database and the International Energy Agency (IEA). This detailed calibration enhances the model's alignment with empirical data, improving the robustness and precision of simulations across sectors and timeframes. AIM-Hub model allows us to quantified emissions of GHGs and various major air pollutants across multiple scenarios which play a critical role in atmospheric chemistry, influencing the formation of $PM_{2.5}$ and O_3. The derived emissions were influenced by a combination of factors, including food production, consumption patterns, population growth, GDP evolution, and technological advancements.

2.2. Emission inventory

In this study, the AIM-Hub model was used to derive an anthropogenic emission inventory using the shared socioeconomic pathways (SSPs) developed by Fujimori et al. (2017, 2018) as an input. The GHGs were defined by AIM-Hub to include carbon dioxide (CO_2), methane, nitrous oxide, and fluorine gas. The other pollutants were black carbon (BC), carbon monoxide, ammonia, non-methane volatile organic compounds, nitrogen oxides (NO_x), organic carbon, and sulfur oxides (SO_x). The Harmonized Emissions Component (HEMCO) is used for providing the natural emission inventory for simulation (Keller et al., 2014; Lin et al., 2021), which including biogenic emissions sourced from MEGAN (Guenther et al., 2012), NOx emissions from lightning (Murray et al., 2012), dust, sea salt (Weng et al., 2020), soil (Hudman et al., 2012) and volcanic eruptions.

To generate the anthropogenic emission flux grid $0.5^\circ \times 0.5^\circ$ grid resolution format which require for GEOS-Chem model, we applied the AIM Downscaling (AIM-DS) tool, which disaggregated the emissions from a 17-region global inventory outcome from AIM-Hub. The downscaling approach was tailored to different emission sectors, as categorized into three groups. Group 1 emissions, from energy, industry, inland transport, buildings, solvents, and waste sectors, were primarily driven by GDP and population trends. In this context, energy-related emissions are hypothesized to be closely linked to these socioeconomic drivers. Group 2 emissions, originating from agriculture, forestry, and land use, were downscaled in proportion to the base year (2015) emissions. Finally, Group 3 emissions, pertaining to aviation, were downscaled in proportion to the global geographic distribution of total emissions for the base year. These sector-specific downscaling methodologies are elaborated in detail by Fujimori et al. (2017, 2018).

2.3. Experimental design

2.3.1. Target area and spatial resolution

In this study, the selection of target areas across different regions followed a consistent methodology, with China as a notable example. Areas were selected based on the severity of air pollution and various socio-economic factors, including population density and energy intensity. To optimize efficiency and reduce computational time, we introduced a customized nested configuration, as illustrated in Fig. 2. This customization allowed us to extend the simulation capabilities to many additional regions worldwide, which were not originally supported by the standard GEOS-Chem code. For example, in Asia, while the standard code covered all of East Asia, our study tailored the nested-grid simulations to China, Japan, and two additional Southeast Asian domains (Southeast Asia 1 and 2). Here, the initial species concentration at boundary of nested grid target area was taken from the boundary condition outcome of entire global simulation at a coarse resolution ($4.0^\circ \times 5.0^\circ$) as suggested by GEOS-Chem Support Team.

To assess model accuracy across different horizontal spatial distributions, we selected a variety of regions within the nested-grid GEOS-Chem simulation. These regions, including the United States, Canada, the European Union, Japan, China, Thailand, Singapore, and Brazil, were chosen to represent diverse geographical areas and varying scales of anthropogenic emissions, which contribute to $PM_{2.5}$ and tropospheric O_3 precursors. The ground surface concentrations obtained from nested-grid simulations in these regions were then compared with global concentration data simulated by the non-nested-grid model.

We assessed the health and agricultural effects arising from the model outputs of the global and nested-grid simulations. Consequently, the spatial distribution of each pollutant was aggregated to a resolution of $0.5^\circ \times 0.5^\circ$, which corresponded to the data inputs from other sources. The first-order conservative remapping technique was applied as a mapping method.

2.3.2. Emission scenarios

To evaluate the performance of the model, we divided the scenarios into two distinct sets. The first set is the baseline scenario, which assumes that future business activities will remain consistent with those in the base year, 2015. This allows us to assess how the model performs under the assumption that no significant changes in activities occur from the base year onward. We used the 2015 simulation to compare with observational data, which helps us evaluate the accuracy of the model at both global and nested-grid resolutions. This comparison is crucial for understanding the model's performance in replicating present-day conditions and validating its reliability before extending it to future scenarios.

The second set of scenarios is the mitigation scenario, which examines the impact of different anthropogenic emission conditions on air quality. Specifically, we implemented a low greenhouse gas (GHG) emissions scenario that aligns with pathways designed to limit the global average temperature increase to 1.5 °C. By including this scenario, we provide a comprehensive visual representation of the emissions reductions, as shown in Supplementary Material Fig. A1. This figure illustrates the potential effects of reduced emissions on air quality and allows us to evaluate the model's performance under future conditions. This analysis is critical for understanding the broader implications of ambitious climate mitigation efforts on environmental quality and public health outcomes.

For future scenarios, we aim to test whether the global or nested grid simulation approach is applicable under these evolving conditions. This is an important step because it can strengthen our conclusions by revealing whether the model introduces biases in its predictions of future scenarios. Identifying these potential biases is essential for evaluating the model's accuracy and reliability in projecting future conditions. By including future scenarios in this study, we can assess the model's performance across different land-use and climate conditions, providing a more comprehensive understanding of its limitations and strengths. This ensures that the model remains a robust tool for informing long-term environmental and public health policies, especially as they relate to future climate challenges.

Note that the climate change impacts such as temperature and precipitation changes were not included in these two scenarios and thus the meteorological condition is same among the scenarios and years while socio-economic for both scenario is based on SSP2 scenario. The

emissions were then entered into the GEOS-Chem model. We selected the years 2015, 2050, and 2100 for CTM simulations to examine the immediate, medium-term, and long-term effects. Data used in this study are available as detailed in the Data Availability section.

2.3.3. Comparison of model outputs with monitoring station observations

To evaluate the results of the GEOS-Chem model, observation data from developed and developing countries (Table 1 and Fig. 3) were compared using 2015 as the baseline year. Due to restricted access to data from ground monitoring stations in certain locations observational data were highly limited.

In the process of comparing observational data with modeled concentrations, the observation point within the target region was assigned to its corresponding grid cell. To assess the accuracy of the model, we utilized monthly average concentration data and computed the mean absolute error (MAE) and the correlation coefficient (R) between the observed and modeled concentrations.

2.3.4. Agricultural impacts

We selected the five main global crops, i.e., sugar cane, maize, soybeans, rice, and wheat, to assess the crop production losses due to O_3 exposure. These crops were selected based on the major crop categories used in the AIM-Hub model.

Formula (1) was used to quantify O_3 exposure in each grid. For the assessment of crop production losses, the accumulated dose of ozone over a threshold of 40 ppb (AOT40) was used to indicate the accumulated O_3 exposure during the daytime in the 3 months before harvesting (Sacks et al., 2010; Tai et al., 2014). (AOT40 was estimated over the time period of 08:00 until 19:59 UTC for the vast areas of agricultural land in temperate and tropical zones.

$$AOT40(\text{ppb}) = \sum_{t=1}^{n} \max([O_3]_t - 40, 0)\ (t \in 08:00 - 19:59) \quad (1)$$

While the response function (2) is used to depict the dose–response relationship between the relative crop yield and O_3 exposure to determine the relative crop yield from AOT40. Different coefficients (a and b) were allocated to different crops as shown in Table A.1 in supplementary material (Mills et al., 2007).

$$y = ax + b \quad (2)$$

where x is AOT40 in ppmh and y is the relative yield.

The Lund–Potsdam–Jena managed land 2 crop model was used for the calculation of the potential production volume and regional consolidation, and potential harvestability and land-use data for the major crops in 2015 from Fujimori et al. (2018) were applied. First, the grid yield was calculated by multiplying the production volume grid by the relative yield. The grid yield was then determined by country and divided into 17 regions (Supplementary Material, Table A.1). The relative yields by country were then calculated by comparing aggregated yields with and without O_3 effects.

Table 1
Sources of air quality monitoring data and number of monitoring station.

Country	Organization (Data sources)	Number of monitoring station	
		$PM_{2.5}$	O_3
United States	Clean Air Status and Trends Network (CASTNET), U.S. Environmental Protection Agency Clean Air Markets Division	396	396
Canada	Ministry of the EnvironmentConservation and Parks	39	39
European Union	European Environment Agency	2021	2700
Japan	National Institute for Environmental Studies	1915	1915
China	China National Environmental Monitoring Centre	1482	1482
Thailand	Air4Thai, Pollution Control Department	12	–
Singapore	Pollution Central Department, National Environment Agency	5	–
Korea	Air Korea, Korea Environmenat Corperation	125	125
Brazil	Environmental Company of the State of São Paulo	14	–

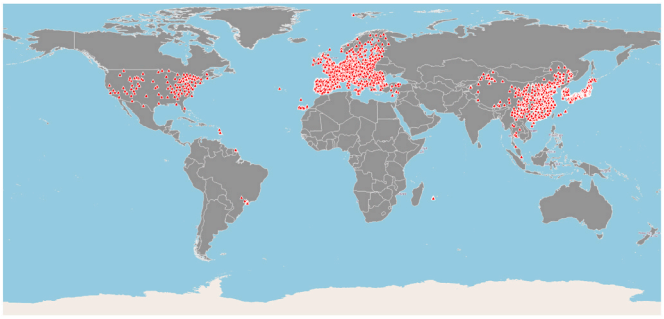

Fig. 3. As shown in Table 1, the spatial distribution mapping of air quality ground monitoring stations.

2.3.5. Mortality due to $PM_{2.5}$ exposure

We also studied the human health impact of $PM_{2.5}$ exposure using the integrated exposure–response (IER) function established by Burnett et al. (2014). The IER function is a nonlinear function that calculates excess mortality due to long-term exposure to ambient $PM_{2.5}$.

We used the Global Burden of Disease tool to provide the specific causes of death following exposure to ambient air pollution. Ischemic heart disease, cerebrovascular illness, acute lower respiratory tract infection, chronic obstructive pulmonary disease, and lung cancer were the target disorders, and data from cohort studies from several countries with varying $PM_{2.5}$ concentrations for these diseases were integrated. Formula (3) expresses the relative risk (RR) due to ambient $PM_{2.5}$ exposure. The IER was established for $PM_{2.5}$ concentrations surpassing C_0 (7.5 μg/m^3), as concentrations lower than 7.5 have not shown any significant association with mortality in cohort studies

$$RR_j(C_i) = 1 + a(1 - \exp(-\beta(C_i - C_0)^{\delta})) \quad (3)$$

where C_i is $PM_{2.5}$ concentration. 'α', 'β', and 'δ' are bare constants in the IER that are age- and disease-specific (j) as shown in Table A.2 in supplementary material.

Mortality was calculated using the RR from equation (3) by using following formula (Apte et al., 2015).

$$Mortality = \frac{RR(z) - 1}{RR(z)} \times Pop \times B \quad (4)$$

where z is the $PM_{2.5}$ concentration (μg/m^3), Pop is grid population (number of people), and B is the baseline mortality rate by country (%).

In this study, we used gridded population estimates based on the SSP2 scenario for both present-day and future scenarios (Jones and O'Neill, 2016). The estimated deaths attributed to $PM_{2.5}$ exposure for all diseases were calculated by combining the death counts for each disease after grouping them by regional divisions.

3. Results

3.1. Spatial distribution of tropospheric O_3 and $PM_{2.5}$ concentrations representation in nested-grid simulations under present-day and future scenario

Fig. 4a illustrates the spatial distributions of O_3 and $PM_{2.5}$ concentrations in nested-grid simulations, demonstrating significant improvements in model performance and the ability to capture localized pollution hotspots compared to global-grid simulations. The global-grid

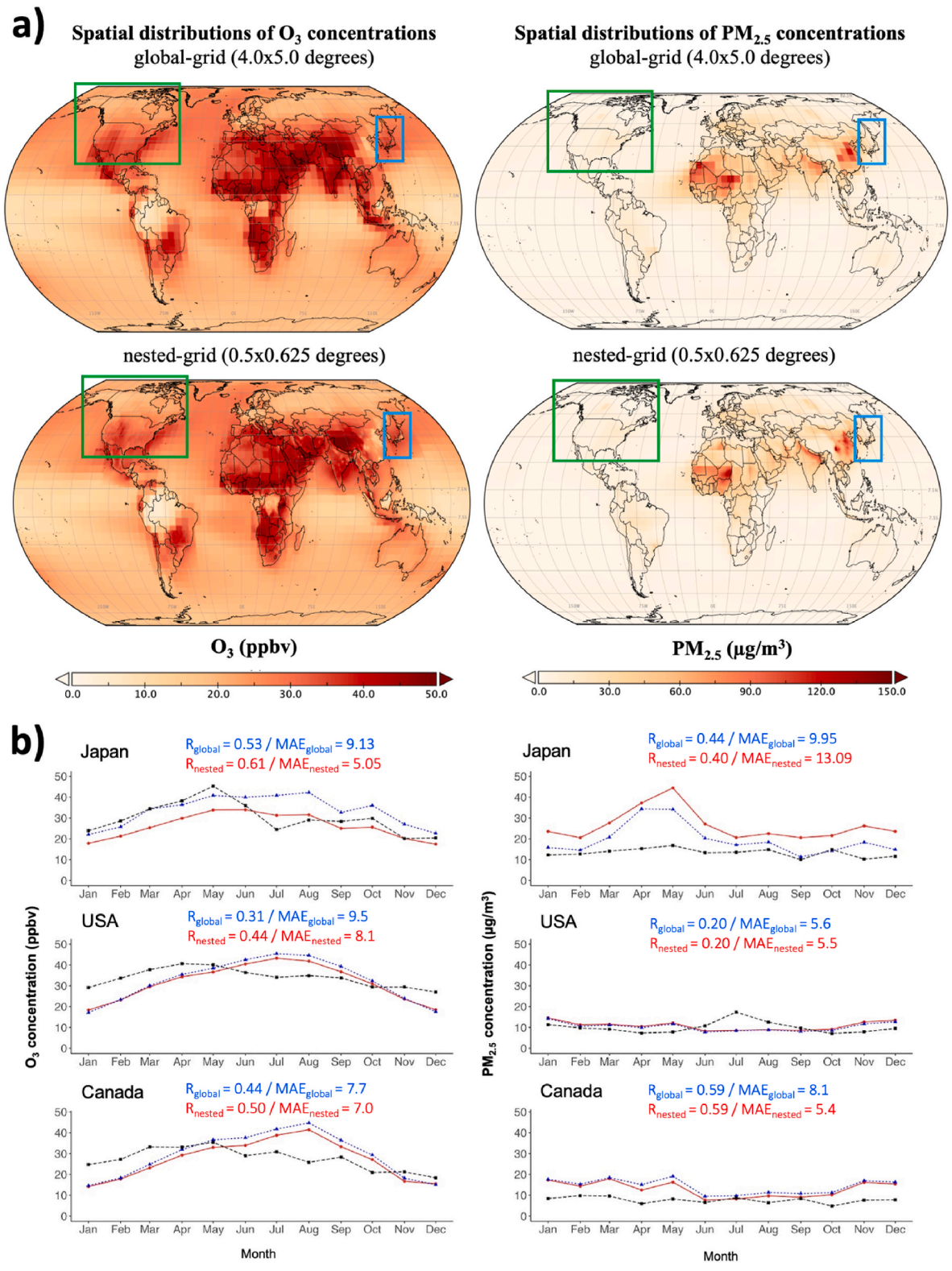

Fig. 4. (a) Spatial distributions of O_3 and $PM_{2.5}$ concentrations simulated using global (upper) and nested (lower) grid simulation under baseline scenario in 2015 (the blue box represents Japan, while green box corresponds to USA and Canada); (b) Monthly O_3 and $PM_{2.5}$ concentrations comparing ground-based observations (black line), global grid simulation with coarse resolution (blue line), and nested-grid simulation (red line) for Japan, the USA, and Canada in 2015. (For interpretation of the references to colour in this figure legend, the reader is referred to the Web version of this article.)

simulations (4.0° × 5.0° resolution) provide a broad and generalized view, often missing finer details of regional pollution patterns. In contrast, nested-grid simulations (0.5° × 0.625° resolution) capture substantial spatial variability, enhancing the representation of local pollution dynamics, particularly in high-pollution regions.

This improved spatial resolution is essential for assessing the model's ability to capture the complexities of air quality responses under present-day and future emission scenarios. For example, while global

grids show widespread elevated $PM_{2.5}$ levels across South Asia, East Asia, and the Middle East, they fail to accurately depict smaller-scale pollution sources and localized emissions. The nested-grid simulations address these gaps by providing enhanced granularity, thereby allowing for a more precise representation of localized emissions and pollution transport mechanisms.

In the present-day (2015) nested-grid simulations, annual average tropospheric O3 concentrations of 30 ppbv or more are observed across extensive regions of the Northern Hemisphere's mid-latitudes, particularly in Asia, Africa, and the Middle East. Notably, high concentrations exceeding 50 ppbv are found over the Tibetan Plateau and parts of central Africa. The elevated O_3 levels in the Tibetan Plateau can be attributed to its high altitude, which enhances the atmospheric column and increases exposure to ultraviolet radiation, promoting ozone formation. In central Africa, high O_3 concentrations are largely due to emissions of volatile organic compounds from widespread vegetation burning, both anthropogenic and natural. For $PM_{2.5}$ concentrations, the nested-grid simulations indicate annual averages surpassing 30 $\mu g/m^3$ across large areas of Asia and Africa, with severe pollution observed in China and India, where levels reach or exceed 120 $\mu g/m^3$. High $PM_{2.5}$ concentrations are also evident in African desert regions, reflecting the inclusion of naturally derived emissions, such as dust, in the simulations.

Moreover, we found that Organic Aerosol (OA), Organic Carbon (OC) and Nitrate (NIT) are better represented in nested high-resolution models compared to low-resolution models, as shown in Figure A.4 of the supplementary material. The nested high-resolution approach captures local meteorological phenomena, such as temperature inversions, local wind patterns, and boundary layer dynamics, with greater accuracy, leading to improved simulations of pollutant dispersion and concentration. These meteorological factors play a significant role in the spatial distribution of OA, OC, and NIT (Wang et al., 2015; Ye et al., 2017; Chen et al., 2024).

A similar spatial distribution pattern of tropospheric O_3 and $PM_{2.5}$ concentrations is observed in the future scenarios for 2050 under both baseline and mitigation conditions (Fig. 5). Elevated O_3 concentrations continue to be prominent over the Tibetan Plateau and central Africa, highlighting the persistent influence of altitude-related factors and regional emissions of ozone precursors, respectively. Similarly, high $PM_{2.5}$ levels remain in Asia, particularly in China and India, as well as in desert regions of Africa, underscoring the ongoing impact of anthropogenic activities and natural sources like dust in these regions.

Fig. 5 projects the spatial distribution of O_3 and $PM_{2.5}$ concentrations for the year 2050 under both baseline and mitigation scenarios using nested-grid simulations. The future scenario analysis underscores the spatial variability of air quality responses to mitigation efforts, revealing that while there are improvements in $PM_{2.5}$ concentrations under mitigation scenarios, reductions are modest, and pollution hotspots persist.

3.2. Model validation for present-day scenario

The daily and monthly mean average data for the grids corresponding to the observation points were used to compare the observation data to the modeling outcomes. This approach ensures that the comparison is made between the model's daily and monthly means and the corresponding observed data, allowing for a direct and accurate evaluation; however, in the European Union and Brazil, only annual average observation data could be obtained due to the limited data accessibility. The observed O_3 (left) and $PM_{2.5}$ (right) concentrations on a monthly scale are shown in Fig. 4b.

The nested-grid simulation for tropospheric ozone provided a modest enhancement in the performance of the model. As shown in Table 2, the Mean Absolute Error (MAE) was reduced while the correlation coefficient (R) was marginally improved in all regions. In Japan, the nested grid simulation leads to a slight decline in MAE and a marginally increase in R for both monthly and daily estimation. However, in Canada, while the nested grid simulation results in a slightly lower MAE, there is no notable improvement in R for daily.

The efficiency of the nested-grid simulation in enhancing the performance of the model for $PM_{2.5}$ estimation varied by region. While some locations showed tremendous improvement, others displayed little or no change (Table 3). In the United States, the nested grid simulation resulted in a marginally reduced MAE for both monthly and daily estimates, but in R, no meaningful improvement was observed (Fig. 4c). Even if Canada's MAE was reduced, R did not improve substantially. Nevertheless, nested-grid simulation does not significantly improve the model's overall performance in compared to non-nested grid simulation. Moreover, in many regions, such as China, Japan, and Korea, the R was improving while the MAE was declining.

With the application of the nested-grid simulation, the estimated $PM_{2.5}$ concentrations in the 2015 data set had a tendency to be overestimated compared to the observations while the nested-grid simulations for O_3 generally provided more accurate results than the global-grid simulations, with lower O_3 levels compared to global-scale simulations, resulting in increased correlation (R) and decreased mean

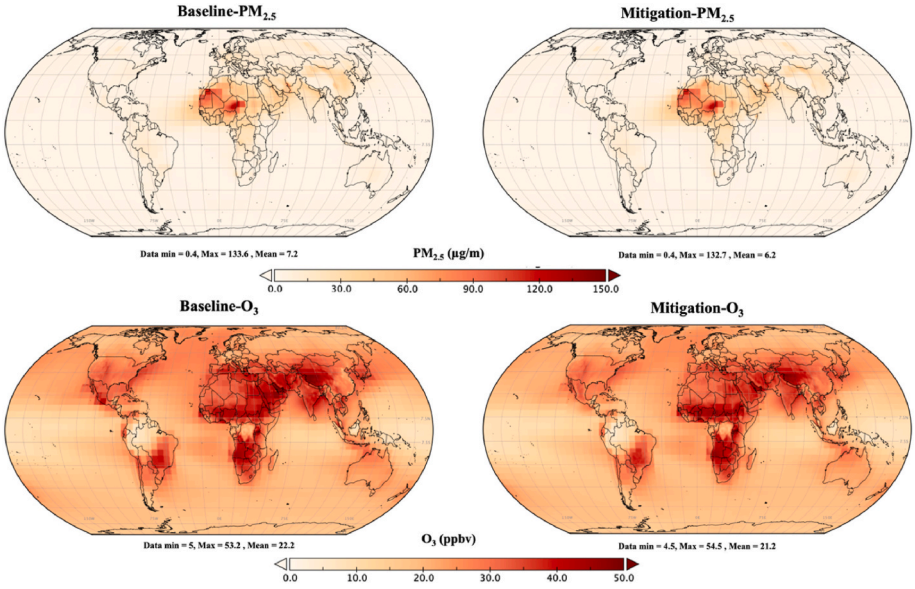

Fig. 5. Projected global distribution (nested-grid simulation) of $PM_{2.5}$ and O_3 concentrations in 2050 under Baseline (left) and Mitigation (right) scenarios.

Table 2
Changes in the MAE and R due to the nested-grid simulation of the modeled/observed O_3 concentrations (ppbv).

Region	Monthly				Daily			
	Global grid		Nested grid		Global grid		Nested grid	
	MAE	R	MAE	R	MAE	R	MAE	R
United States	9.5	0.31	8.1	0.44	11.2	0.26	10.6	0.31
Japan	9.13	0.53	5.05	0.61	10.85	0.25	10.78	0.31
Canada	7.7	0.44	7.0	0.50	10.3	0.29	9.7	0.30
European Union[a]	6.1	0.29	5.8	0.33	–	–	–	–
China	31.45	0.39	30.82	0.56	30.03	0.42	32.71	0.41
Korea	8.12	0.68	5.05	0.73	–	–	–	–

[a] Annual average.

Table 3
Changes in the MAE and R due to the nested-grid simulation of the modeled/observed $PM_{2.5}$ concentration ($\mu g/m^3$).

Region	Monthly				Daily			
	Global grid		Nested grid		Global grid		Nested grid	
	MAE	R	MAE	R	MAE	R	MAE	R
United States	5.6	0.20	5.5	0.20	6.2	0.11	6.4	0.13
Japan	9.95	0.44	13.09	0.40	10.0	0.26	15.3	0.21
Canada	8.1	0.59	5.4	0.59	8.3	0.19	7.5	0.2
China	27.67	0.43	29.1	0.53	36.80	0.23	38.27	0.27
Thailand	12.9	0.55	13.2	0.54	15.1	0.36	17.2	0.38
Singapore	14.1	0.16	13.9	0.38	14.4	0.05	14.3	0.20
Korea	8.13	0.32	21.3	0.38	–	–	–	–
European Union[a]	12.2	0.37	9.7	0.38	–	–	–	–
Brazil[a]	15.2	0.44	19.3	0.46	–	–	–	–

[a] Annual average.

absolute error (MAE) when compared to observations (Fig. 4b). The overall O_3 concentration was overestimated by around 3.5 ppbv (11.8%) on a monthly basis, whereas the $PM_{2.5}$ concentration was overestimated by approximately 20.9 $\mu g/m^3$ (122%). For daily investigations, the result was a 12% (3.6 ppbv) overestimation of the O_3 concentration and a 97.7% (13.0 $\mu g/m^3$) overestimation of the $PM_{2.5}$ concentration. This result is related to Travis et al. (2016) study. Their study revealed that the CTM model's surface ozone concentrations exhibited an overestimation, attributed to a combination of heightened vertical mixing and net ozone production within the model's boundary layer. In the context of $PM_{2.5}$ concentration, the GEOS-Chem model demonstrates a tendency to overstate levels of nitrate, elemental carbon (EC), and organic carbon (OC). This overestimation collectively contributes to an overall exaggeration in $PM_{2.5}$ concentration estimates. (Lee et al., 2017).

In terms of seasonal variation, the reproducibility of the O_3 concentration was generally good and the geographical characteristics were also well reproduced (Fig. 4a-right). However, in the nested-grid simulation, the estimated concentration was close to the observed data only in Japan and the European Union, while there was a decrease in the MAE in all regions (Fig. 4b). The influence of the nested-grid simulation on the validity of the modeled concentrations was therefore considered to be limited.

The seasonal repeatability of $PM_{2.5}$ was equivalent to that of O_3. The MAEs of the estimated and observed concentrations were lowest in Canada, Singapore, and the European Union, with values of 2.7 $\mu g/m^3$ for monthly data and 0.8 $\mu g/m^3$ for daily data. In contrast to the overestimation that occurred in the majority of locations, the difference between the modeled and observed concentration and the MAE were minor when the nested-grid simulation was applied. Despite the fact that nested grid could improve the result's precision in comparison to non-nested grid, the overall performance of both models is poor. The models may not adequately represent the complexity of atmospheric processes that influence air quality, which is the leading cause of model uncertainty such as regional meteorological pattern.

3.3. *p.m.$_{2.5}$ exposure and mortality for future scenario*

Fig. 6a compares premature deaths caused by $PM_{2.5}$ exposure between nested-grid and global-grid simulations. In the baseline year (2015), both simulations predict similar global mortality rates of about 5 million deaths, with only minor discrepancies. However, in future scenarios, the nested-grid simulations consistently estimate higher premature deaths compared to the global-grid simulations. For example, in 2050, the nested-grid simulation forecasts around 4.5 million deaths under the baseline scenario, compared to about 4 million in the global grid—a difference of approximately 0.5 million deaths. This gap widens by 2100, even under the mitigation scenario where emissions reductions are implemented, indicating that nested-grid simulations continue to show higher mortality rates.

The purpose of including future scenario simulations was not just to confirm the existence of resolution-induced discrepancies in health and environmental impact estimates, but to illustrate how these discrepancies may evolve over time and under different emission reduction scenarios. The results show that the differences between the nested and global simulations are due to the nested grid's finer resolution, which more accurately captures local pollution sources and dispersion patterns, particularly in densely populated and industrialized regions as mentioned in section 3.1. This is especially relevant in future scenarios where emission reductions are unevenly distributed across regions.

The nested-grid simulations predict significantly higher pollutant concentrations in regions like China and India because they provide a more detailed representation of local dynamics, including hotspots of urban and industrial emissions, which the coarser global grid averages out. Interestingly, even in mitigation scenarios, the nested grid shows lower estimates of deaths in some years compared to the global grid, suggesting that nested grids are more sensitive to spatially uneven emission reductions and can better capture localized improvements in air quality that the global grid might miss.

Fig. 6b further explores regional differences in predicted deaths between nested and global grid simulations through scatterplots. In both

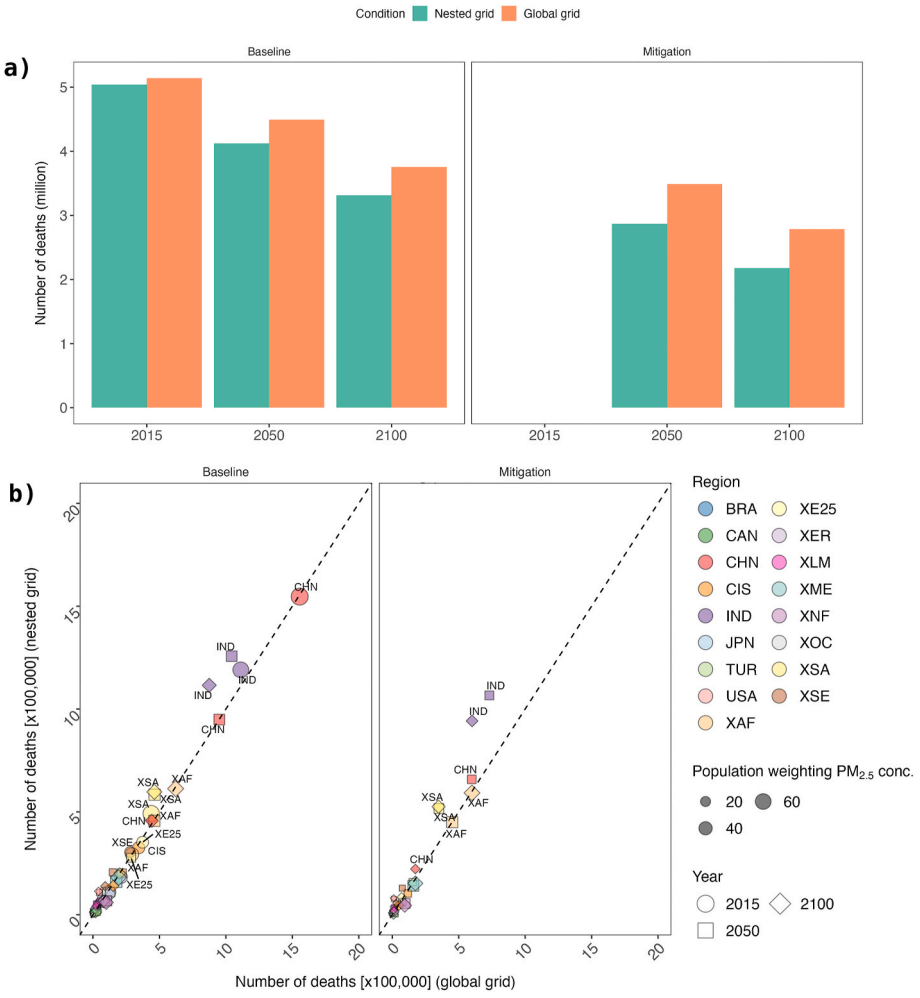

Fig. 6. (a) Comparison of the number of worldwide premature deaths attributable to exposure to $PM_{2.5}$ between the global (orange) and nested (green) grid simulations. (b) Changes in the number of deaths by region due to the application of the nested-grid simulation (the black diagonal represents the 1:1 line). BRA = Brazil; CAN = Canada; CHN = China; CIS = Former Soviet Union; IND = India; JPN = Japan; TUR = Turkey; USA = United States of America; XAF = Sub-Saharan; XER = Europe (excluding the European Union); XE25 = European Union (EU25); XLM = Latin America; XME = Middle East; XNF = North Africa; XOC = Oceania; XSA = Rest of Asia; XSE = Southeast Asia. Each point represents a region, with the x-axis indicating deaths from the global grid and the y-axis from the nested grid. The size of the points reflects population-weighted $PM_{2.5}$ concentration, highlighting regions where higher exposure contributes more significantly to mortality rates. (For interpretation of the references to colour in this figure legend, the reader is referred to the Web version of this article.)

baseline and mitigation scenarios, regions with points above the diagonal line indicate that nested-grid simulations predict more deaths than global-grid simulations, emphasizing the discrepancy between the two approaches. This difference is particularly pronounced in rapidly developing regions such as China (CHN), India (IND), and Southeast Asia (XSA), where high population density and industrial activity lead to concentrated emissions. For instance, in India, the nested-grid simulation shows significantly higher predicted deaths in 2050 and 2100 compared to the global grid, underscoring the importance of capturing localized pollution dynamics that influence public health outcomes.

The regional analysis shows that these discrepancies are not uniformly distributed; they are amplified in areas with high emissions and dense populations. This means the nested grided resolution provides a more accurate picture of pollution exposure, which is crucial for planning effective public health interventions. Moreover, the increasing discrepancies in future mitigation scenarios suggest that the nested grids are more responsive to uneven reductions in emissions, highlighting areas where pollutant levels may remain high despite overall decreases in emissions. This underscores the need for high-resolution modeling in future impact assessments to ensure that mitigation strategies are appropriately targeted to areas that remain at risk.

3.4. Crop production losses due to O_3 exposure for future scenario

Fig. 7a illustrates the relative yield loss percentages due to ozone exposure for the years 2015, 2050, and 2100 under both baseline and mitigation scenarios, comparing nested-grid and global-grid simulations. In the base year of 2015, the global relative yield loss was approximately 7%, with nested-grid simulations showing slightly higher losses compared to global-grid simulations. The discrepancies between nested and global grids become more pronounced in future scenarios. By 2050, the nested-grid simulations project a relative yield loss of around 5% under the baseline scenario, while the global grid predicts a slightly lower loss of about 4.5%. This gap widens further by 2100, particularly under the mitigation scenario, where the nested grid continues to estimate higher yield losses than the global grid, indicating that the nested grid captures localized ozone exposure more sensitively than global grid simulation.

The discrepancies between nested and global grid simulations can be attributed to the finer spatial resolution of the nested grid, which allows it to better capture local emission sources and ozone formation dynamics, particularly in high-emission regions such as the Middle East, India, and Southeast Asia. This detailed representation is crucial in areas where ozone concentrations are highly variable and can lead to localized

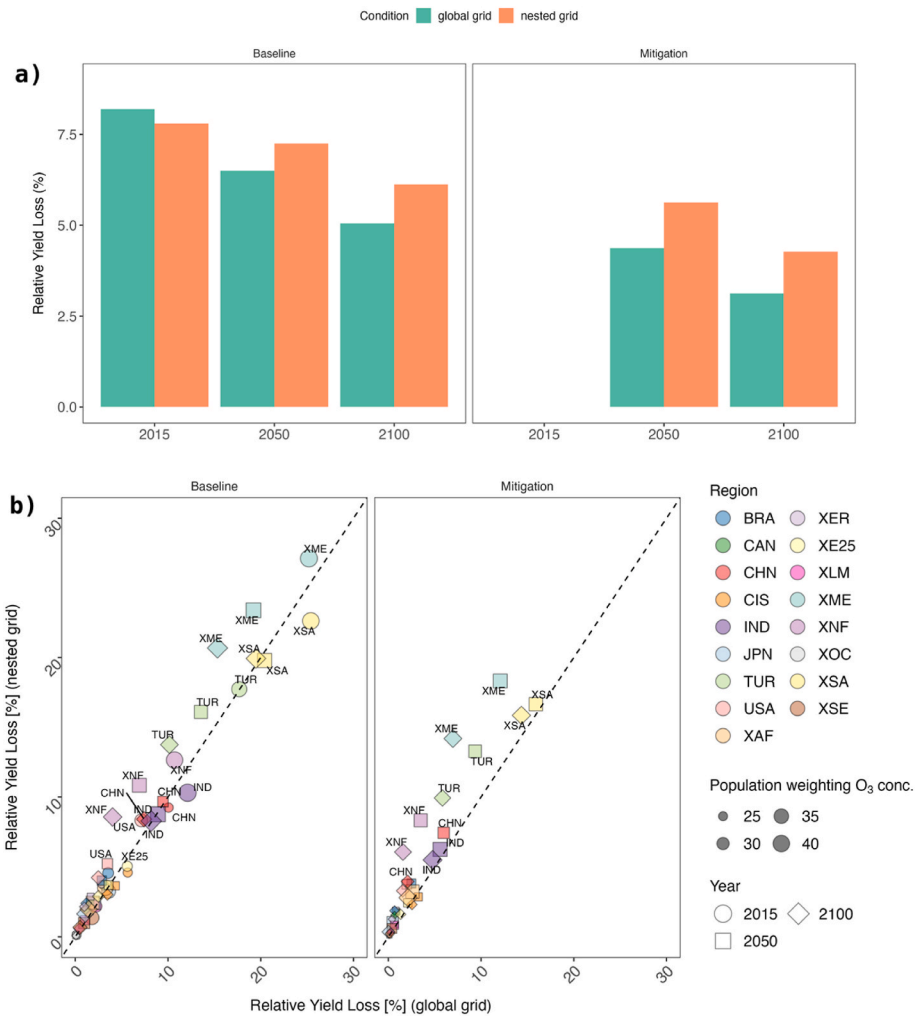

Fig. 7. (a) Comparison of the worldwide crop production loss due to O_3 exposure in the simulations with and without nested grids; (b) Changes in crop production loss by region due to the application of the nested-grid simulation (the black diagonal represents the 1:1 line). Each point represents a region, with the x-axis indicating deaths from the global grid and the y-axis from the nested grid. The size of the points reflects population-weighted O_3 concentration.

spikes that impact crop yields significantly. In regions with high agricultural productivity, such as the United States and the European Union, the nested grid predicts slightly higher yield losses (by 1–2%) due to its ability to capture localized ozone hotspots that the global grid averages out.

Fig. 7a shows a scatterplot comparing relative yield loss by region between nested and global grid simulations. Notably, the differences are most pronounced in the Middle East (XME) and neighboring regions like Turkey (TUR) and North Africa (XAF), where the nested grid predicts up to 7% higher losses compared to the global grid, especially in future scenarios. This discrepancy is likely due to the nested grid's sensitive capability to resolve high local concentrations of ozone that are less visible in the coarser global grid simulations as shown in Fig. 4a.

4. Discussion

4.1. Trans-boundary conditions

In this study, we have implemented adjustments to the nested-grid methodology to enhance the efficiency of computationally demanding tasks, such as running high-resolution simulations over multiple regions and processing observational data for model evaluation (refer to Fig. 2). The nested-grid simulations conducted in the nested-Asia region, including SEA1, SEA2, CHN, and JPN, were evaluated to assess their effectiveness under this customized configuration.

Through a comparative analysis, we juxtaposed the validation results derived from these simulations with those obtained from the custom nested approach utilized in our research. Notably, our findings indicate that there are no significant disparities between the outcomes of both nested-Asia and custom nested simulations, particularly evident in the contexts of O_3 concentrations in Japan and China, and $PM_{2.5}$ levels across Japan, China, Korea, Thailand, and Singapore, as illustrated in Table A3 and Fig. A3 of the supplement material.

However, in Korea, we discovered that utilizing nested-Asia could yield a higher correlation between model outcomes and observational data compared to nested-custom (JPN), particularly regarding O_3 concentrations. This finding aligns with the study by Colombi et al. (2023), which concluded that simulating ozone concentrations in Korea is challenging due to transboundary influences.

4.2. Impact assessment

We compare the agricultural impact assessment of our study with Van Dingenen et al. (2009). We found that while the relative crop yield loss trend was consistent when accounting for differences in target years and crop definitions, regional discrepancies were notable, particularly in the Middle East, where crop production losses have increased due to high emission loads since 2005. Specifically, nested-grid calculations showed a 1% difference in global average relative yield loss and a 7% difference in regional areas compared to Van Dingenen et al. (2009).

Although these differences are relatively minor globally, they could have significant implications for food supply and economic systems at regional scales.

Regarding health impacts, our model overestimated mortality related to $PM_{2.5}$ exposure, with an overestimate of 5.2 million for nested and 5 million for non-nested simulations, compared to the WHO's reported 4.2 million deaths in 2015. This suggests that, within our specific model configuration including GEOS-Chem model physics and chemistry, meteorological data, and emissions, the global grid simulation aligns more closely with observed data. However, it is important to emphasize that these findings are contingent upon the specific parameters and conditions of our study, underlining the need for detailed model evaluations to ensure accuracy across varying scenarios.

Furthermore, our analysis indicates that nested-grid simulations, which operate at higher spatial resolutions, are more sensitive to pollutant concentrations and thus exert a stronger influence on impact assessments compared to global grid simulations. This increased sensitivity, critical for capturing fine-scale atmospheric processes such as localized emissions and complex terrain effects, becomes particularly significant in regions with high emission densities or complex environmental conditions. Conversely, the lower spatial resolution of global grid simulations may smooth out these variations, potentially leading to less precise assessments of pollutant concentrations and their impacts (Wang et al., 2011; Punger and West, 2013).

4.3. Limitation

The observed overestimations in modeled O_3 and $PM_{2.5}$ concentrations compared to observed levels, across both global and nested-grid simulations, suggest that increasing spatial resolution does not necessarily improve model accuracy. This consistent overestimation points to intrinsic limitations within the model's performance, potentially stemming from inaccuracies in the emission inventories, chemical mechanisms, or boundary conditions used in the simulations. The findings underscore the limited impact of nested-grid simulations on enhancing the precision of modeled concentrations, highlighting the necessity for further refinement of model inputs and processes to improve reliability.

Moreover, the study reveals that while the global and regional impacts on health effect calculations were less pronounced, the agricultural impacts demonstrated significant regional variations. This suggests that agricultural impacts, in particular, may be subject to considerable changes in the future. It is crucial to incorporate model uncertainties when evaluating regional effects of air pollution on agriculture, as these uncertainties can significantly influence the study's conclusions. Even though global assessments using low-resolution models maintained the reliability of outcomes, these models were less effective at accurately replicating daily data, as shown in Table 2, though they were competent at capturing broader temporal trends. This highlights the importance of selecting appropriate model resolutions tailored to the specific application, particularly when assessing localized or short-term impacts.

Several limitations of this study must be acknowledged. Firstly, the results are dependent on the specific parameters used within the GEOS-Chem model. While GEOS-Chem's high-resolution meteorological conditions and terrain are precise within nested regions, it cannot simulate all atmospheric phenomena that may occur. Secondly, the simulations did not include interactions between air pollutants and meteorological conditions; GEOS-Chem uses meteorological data as input without allowing feedback from air pollutants. For example, aerosol processes that block solar radiation were not considered, which could affect atmospheric dynamics and pollutant levels. Thirdly, high-resolution nested-grid simulations use global grid concentrations as boundary conditions, introducing potential dependencies on transboundary pollution effects. This is a known limitation of the GEOS-Chem model, which relies on global simulations to provide boundary conditions for nested domains. If the global model inaccurately represents transboundary pollution or fails to capture the variability and dynamics of pollutants near the boundaries, these errors can propagate into the nested simulations. As a result, the nested-grid simulations may inherit biases from the global model, which can diminish the expected improvements in accuracy from higher spatial resolution. This limitation underscores the need for careful evaluation and potential adjustments to boundary conditions in nested-grid configurations to mitigate the influence.

Additionally, the emission inventory used in this study, particularly when evaluating long-term impacts of land cover and land use changes, introduces additional uncertainties. The downscaling method from the AIM-Hub model scales emissions based on regional totals within the agricultural sector using the CEDS emission grid. This approach may not fully account for the complexities of land cover and land use changes over time, potentially overlooking localized variations and specific land use dynamics, which contributes to uncertainties in the emissions data.

5. Summary and conclusions

This study assessed the impacts of air pollution on agriculture and human health using global and nested-grid simulations of O_3 and $PM_{2.5}$ concentrations with the GEOS-Chem model under multiple future emission scenarios. Our analysis revealed that while nested-grid simulations enhanced spatial resolution, they did not significantly improve the overall accuracy of modeled pollutant concentrations compared to global grid simulations, as observed in the base year comparisons across different horizontal resolutions. However, nested-grid simulations provided better alignment with observed data on monthly and daily scales, particularly in regions like the United States and European Union, due to a more accurate representation of meteorological complexities affecting pollutant distributions.

Impact assessments showed that estimated yield loss and mortality rates were consistent with existing literature, with nested-grid simulations predicting a global increase in mortality by approximately 10,000 cases compared to non-nested simulations. While this difference fell within the margin of error, it underscores the potential impact of higher spatial resolution on local assessments. Regionally, significant variations were noted, especially in Asia, where mortality rates fluctuated by up to 500,000 deaths, although these changes represented a minor fraction of the total population. For agricultural impacts, nested-grid simulations indicated a global yield loss reduction of around 7%, with specific reductions in Asia and increases in the Middle East and high-production regions like the United States and European Union. Despite these regional shifts, the overall global yield loss remained stable due to the balancing effect of varied regional responses.

Our findings highlight that while nested-grid simulations offer enhanced sensitivity to pollutant concentrations, capturing fine-scale atmospheric processes crucial in high-emission or complex regions, they also exhibit consistent overestimations in O_3 and $PM_{2.5}$ concentrations. This suggests that increased spatial resolution alone is insufficient to improve model accuracy, emphasizing the need for refining emission inventories, chemical mechanisms, and boundary conditions in the simulations. The study also identified the inherent dependency of nested-grid simulations on global boundary conditions, which can propagate biases from global models into regional analyses.

The modest impact of CTM resolution on yield losses and mortality, with generally lower estimates in non-nested simulations, particularly under mitigation scenarios, underscores the importance of incorporating model uncertainties in evaluating mitigation strategies. The most pronounced differences between nested and non-nested simulations occurred in the mitigation scenario, reinforcing the need to carefully consider model resolution choices in policy assessments.

These results are specific to the study's configuration, including the GEOS-Chem model setup, selected meteorological data, and emission inventories. Therefore, the conclusions should not be generalized across all studies and scenarios without thorough evaluation of alternative model configurations and parameters. Future research should explore

diverse configurations and conduct detailed evaluations to better understand the broader implications of horizontal resolution choices in nested-grid simulations, particularly their impact on agricultural and health assessments across various regions and emission scenarios.

CRediT authorship contribution statement

Thanapat Jansakoo: Writing – original draft, Visualization, Validation, Methodology, Conceptualization. **Ryouichi Watanabe:** Writing – original draft, Visualization, Validation, Methodology, Conceptualization. **Akio Uetani:** Writing – original draft, Visualization, Validation, Methodology. **Satoshi Sekizawa:** Methodology, Formal analysis. **Shinichiro Fujimori:** Writing – review & editing, Conceptualization. **Tomoko Hasegawa:** Writing – review & editing. **Ken Oshiro:** Writing – review & editing.

Code availability

GEOS-Chem (GCClassic) version 12.9.3 code is available from https://github.com/geoschem/geos-chem. The source code of the crop model (LPJmL) is available under the AGPLv3 license at https://github.com/PIK-LPJmL/LPJmL.

Declaration of generative AI and AI-assisted technologies in the writing process

During the preparation of this work the author(s) used ChatGPT in order to improve the clarity and coherence of writing and for grammar checking. No AI was employed for conceptual or substantive content generation, data analysis, or decision-making processes related to the research. After using this tool, the author(s) reviewed and edited the content as needed and take(s) full responsibility for the content of the publication.

Declaration of competing interest

The authors declare that they have no known competing financial interests or personal relationships that could have appeared to influence the work reported in this paper.

Acknowledgments

This research was financially supported by the Environment Research and Technology Development Fund (JPMEERF20241001) of the Environmental Restoration and Conservation Agency of the Japanese Ministry of Environment, Japan Science and Technology Agency (JST) as part of Adopting Sustainable Partnerships for Innovative Research Ecosystem (ASPIRE), Grant Number JPMJAP2331, and by the Sumitomo Electric Industries Group CSR Foundation. A portion of this research was conducted using a supercomputer at the Academic Center for Computing and Media Studies, Kyoto University.

Appendix A. Supplementary data

Supplementary data to this article can be found online at https://doi.org/10.1016/j.aeaoa.2024.100303.

Data availability

The scenario data, emission flux, and outcomes from the GEOS-Chem model are available for access via the following link: https://doi.org/10.7910/DVN/APZ0CG.

References

Agrawal, M., 2005. Effects of air pollution on agriculture: an issue of national concern. Natl. Acad. Sci. Lett. 28 (3/4), 93–106.

Anenberg, S.C., Horowitz, L.W., Tong, D.Q., West, J.J., 2010. An estimate of the global burden of anthropogenic ozone and fine particulate matter on premature human mortality using atmospheric modeling. Environ. Health Perspect. 118 (9), 1189–1195. https://doi.org/10.1289/ehp.0901220.

Apte, J.S., Marshall, J.D., Cohen, A.J., Brauer, M., 2015. Addressing global mortality from ambient PM2. 5. Environ. Sci. Technol. 49 (13), 8057–8066.

Ashmore, M., 1991. Air pollution and agriculture. Outlook Agric. 20 (3), 139–144.

Askariyeh, M.H., Khreis, H., Vallamsundar, S., 2020. Air pollution monitoring and modeling. In: Traffic-Related Air Pollution. Elsevier, pp. 111–135.

Bey, I., Jacob, D.J., Yantosca, R.M., Logan, J.A., Field, B.D., Fiore, A.M., Li, Q., Liu, H.Y., Mickley, L.J., Schultz, M.G., 2001. Global modeling of tropospheric chemistry with assimilated meteorology: model description and evaluation. J. Geophys. Res. Atmos. 106 (D19), 23073–23095. https://doi.org/10.1029/2001JD000807.

Brunekreef, B., Holgate, S.T., 2002. Air pollution and health. Lancet 360 (9341), 1233–1242.

Burnett, R.T., Pope III, C.A., Ezzati, M., Olives, C., Lim, S.S., Mehta, S., Shin, H.H., Singh, G., Hubbell, B., Brauer, M., 2014. An integrated risk function for estimating the global burden of disease attributable to ambient fine particulate matter exposure. Environ. Health Perspect. 122 (4), 397–403. https://doi.org/10.1289/ehp.1307049.

Chen, D., Wang, Y., McElroy, M.B., He, K., Yantosca, R.M., Le Sager, P., 2009. Regional CO pollution and export in China simulated by the high-resolution nested-grid GEOS-Chem model. Atmos. Chem. Phys. 9 (11), 3825–3839. https://doi.org/10.5194/acp-9-3825-2009.

Chen, Q., Miao, R., Geng, G., Shrivastava, M., Dao, X., Xu, B., et al., 2024. Widespread 2013-2020 decreases and reduction challenges of organic aerosol in China. Nat. Commun. 15 (1), 4465.

China National Environmental Monitoring Centre. (n.d.), Air quality monitoring data report, Retrieved April 18, 2022 from, https://quotsoft.net/air/.

Chuwah, C., van Noije, T., van Vuuren, D.P., Stehfest, E., Hazeleger, W., 2015. Global impacts of surface ozone changes on crop yields and land use. Atmos. Environ. 106, 11–23. https://doi.org/10.1016/j.atmosenv.2015.01.062.

Cissé, G., McLeman, R., Adams, H., Aldunce, P., Bowen, K., Campbell-Lendrum, D., Clayton, S., Ebi, K., Hess, J., Huang, C., 2022. Health, wellbeing, and the changing structure of communities. Clim 2022, 1041–1170.

Cohen, A.J., Brauer, M., Burnett, R., Anderson, H.R., Frostad, J., Estep, K., Balakrishnan, K., Brunekreef, B., Dandona, L., Dandona, R., 2017. Estimates and 25-year trends of the global burden of disease attributable to ambient air pollution: an analysis of data from the Global Burden of Diseases Study 2015. Lancet 389 (10082), 1907–1918. https://doi.org/10.1016/S0140-6736(17)30505-6.

Environmental Company of the State of São Paulo. (n.d.). Air quality report in the State of São Paulo. Retrieved April 19, 2022, from https://cetesb.sp.gov.br/ar/publicacoes-relatorios/.

European Environment Agency. (n.d.). Air quality statistics calculated by the EEA. Retrieved April 15, 2022, from http://aidef.apps.eea.europa.eu.

Colombi, N.K., Jacob, D.J., Yang, L.H., Zhai, S., Shah, V., Grange, S.K., Liao, H., 2023. Why is ozone in South Korea and the Seoul metropolitan area so high and increasing? Atmospheric Chemistry and Physics 23 (7), 4031–4044.

Fiore, A.M., Naik, V., Leibensperger, E.M., 2015. Air quality and climate connections. J. Air Waste Manag. Assoc. 65 (6), 645–685. https://doi.org/10.1080/10962247.2015.1040526.

Fountoukis, C., Nenes, A., 2007. Isorropia II: a computationally efficient thermodynamic equilibrium model for K+–Ca 2+–Mg 2+–NH 4+–Na+–SO 4 2−–NO 3−–Cl−–H 2 O aerosols. Atmos. Chem. Phys. 7 (17), 4639–4659. https://doi.org/10.5194/acp-7-4639-2007.

Fujimori, S., Abe, M., Kinoshita, T., Hasegawa, T., Kawase, H., Kushida, K., Masui, T., Oka, K., Shiogama, H., Takahashi, K., 2017. Downscaling global emissions and its implications derived from climate model experiments. PLoS One 12 (1), e0169733. https://doi.org/10.1371/journal.pone.0169733.

Fujimori, S., Hasegawa, T., Ito, A., Takahashi, K., Masui, T., 2018. Gridded emissions and land-use data for 2005–2100 under diverse socioeconomic and climate mitigation scenarios. Sci. Data 5 (1), 1–13. https://doi.org/10.1038/sdata.2018.210.

Fujimori, S., Masui, T., Matsuoka, Y., 2012. AIM/CGE [basic] manual. Center for Social and Environmental Systems Research, NIES, Tsukuba, Japan.

Fujimori, S., Wu, W., Doelman, J., Frank, S., Hristov, J., Kyle, P., Takahashi, K., 2022. Land-based climate change mitigation measures can affect agricultural markets and food security. Nature Food 3 (2), 110–121.

Guenther, A.B., Jiang, X., Heald, C.L., Sakulyanontvittaya, T., Duhl, T., Emmons, L.K., Wang, X., 2012. The Model of Emissions of Gases and Aerosols from Nature version 2.1 (MEGAN2.1): an extended and updated framework for modeling biogenic emissions. Geosci. Model Dev. 5, 1471–1492. https://doi.org/10.5194/gmd-5-1471-2012.

Hudman, R., Moore, N., Mebust, A., Martin, R., Russell, A., Valin, L., Cohen, R., 2012. Steps towards a mechanistic model of global soil nitric oxide emissions: implementation and space based-constraints. Atmos. Chem. Phys. 12 (16), 7779–7795. https://doi.org/10.5194/acp-12-7779-2012.

Iwata, H., Okada, K., 2014. Greenhouse gas emissions and the role of the Kyoto Protocol. Environ. Econ. Pol. Stud. 16, 325–342. https://doi.org/10.1007/s10018-012-0047-1.

Jacob, D.J., Winner, D.A., 2009. Effect of climate change on air quality. Atmos. Environ. 43 (1), 51–63. https://doi.org/10.1016/j.atmosenv.2008.09.051.

Jiang, P., Chen, Y., Geng, Y., Dong, W., Xue, B., Xu, B., Li, W., 2013. Analysis of the co-benefits of climate change mitigation and air pollution reduction in China. J. Clean. Prod. 58, 130–137. https://doi.org/10.1016/j.jclepro.2013.07.042.

Jones, B., O'Neill, B.C., 2016. Spatially explicit global population scenarios consistent with the Shared Socioeconomic Pathways. Environ. Res. Lett. 11 (8), 084003. https://doi.org/10.1088/1748-9326/11/8/084003.

Korea Environmenat Corperation. (n.d.). AirKorea. Retrieved April 20, 222 C.E., from https://www.airkorea.or.kr/web/detailViewDown?pMENU_NO=125.

Keller, C.A., Long, M.S., Yantosca, R.M., Da Silva, Pawson, S., Jacob, D.J., 2014. HEMCO v1. 0: a versatile, ESMF-compliant component for calculating emissions in atmospheric models. Geoscientific Model Dev. 7 (4), 1409–1417.

Lee, H.-M., Park, R.J., Henze, D.K., Lee, S., Shim, C., Shin, H.-J., Moon, K.-J., Woo, J.-H., 2017. PM2. 5 source attribution for Seoul in May from 2009 to 2013 using GEOS-Chem and its adjoint model. Environmental Pollution 221, 377–384.

Lin, H., Jacob, D. J., Lundgren, E. W., Sulprizio, M. P., Keller, C. A., Fritz, T. M., Eastham, S. D., Emmons, L. K., Campbell, P. C., Baker, B., Saylor, R. D., and Montuoro, R.: Harmonized Emissions Component (HEMCO) 3.0 as a versatile emissions component for atmospheric models: application in the GEOS-Chem, NASA GEOS, WRF-GC, CESM2, NOAA GEFS-Aerosol, and NOAA UFS models, Geosci. Model Dev., 14, 5487–5506, https://doi.org/10.5194/gmd-14-5487-2021, 2021.

Mao, J., Paulot, F., Jacob, D.J., Cohen, R.C., Crounse, J.D., Wennberg, P.O., Keller, C.A., Hudman, R.C., Barkley, M.P., Horowitz, L.W., 2013. Ozone and organic nitrates over the eastern United States: sensitivity to isoprene chemistry. J. Geophys. Res. Atmos. 118 (19), 11–256. https://doi.org/10.1002/jgrd.50817.

Mills, G., Buse, A., Gimeno, B., Bermejo, V., Holland, M., Emberson, L., Pleijel, H., 2007. A synthesis of AOT40-based response functions and critical levels of ozone for agricultural and horticultural crops. Atmos. Environ. 41 (12), 2630–2643. https://doi.org/10.1016/j.atmosenv.2006.11.016.

Ministry of the Environment, Conservation and Parks. (n.d.). *Air Pollutant Data*. Air Quality Ontario; Government of Ontario, Ministry of the Environment. Retrieved April 13, 2022, from http://www.airqualityontario.com/history/.

Murray, L.T., Jacob, D.J., Logan, J.A., Hudman, R.C., Koshak, W.J., 2012. Optimized regional and interannual variability of lightning in a global chemical transport model constrained by LIS/OTD satellite data. J. Geophys. Res. Atmos. 117 (D20). https://doi.org/10.1029/2012JD017934.

National Environment Agency. (n.d.). *Historical 1-hr PM2.5*. Data.Gov.Sg. Retrieved April 19, 2022, from https://data.gov.sg/dataset/historical-1-hr-pm2-5.

National Institute for Environmental Studies. (n.d.). Environmental Numerical Database. Retrieved April 15, 2022, from https://www.nies.go.jp/igreen/index.html.

Nemet, G.F., Holloway, T., Meier, P., 2010. Implications of incorporating air-quality co-benefits into climate change policymaking. Environ. Res. Lett. 5 (1), 014007. https://doi.org/10.1088/1748-9326/5/1/014007.

Occhipinti, Z., Verona, R., 2020. Kyoto Protocol (KP). Climate Action 605–617. https://doi.org/10.1007/978-3-319-95885-9_23.

O'Neill, B.C., Kriegler, E., Ebi, K.L., Kemp-Benedict, E., Riahi, K., Rothman, D.S., Solecki, W., 2017. The roads ahead: Narratives for shared socioeconomic pathways describing world futures in the 21st century. Global environmental change 42, 169–180.

Parrella, J., Jacob, D.J., Liang, Q., Zhang, Y., Mickley, L.J., Miller, B., Evans, M., Yang, X., Pyle, J., Theys, N., 2012. Tropospheric bromine chemistry: implications for present and pre-industrial ozone and mercury. Atmos. Chem. Phys. 12 (15), 6723–6740. https://doi.org/10.5194/acp-12-6723-2012.

Pollution Control Department, Thailand. (n.d.). Air4Thai: Historical data. Retrieved April 18, 2022, from http://www.air4thai.com/webV2/history/.

Protonotariou, A., Tombrou, M., Giannakopoulos, C., Kostopoulou, E., Le Sager, P., 2010. Study of CO surface pollution in Europe based on observations and nested-grid applications of GEOS-CHEM global chemical transport model. Tellus B 62 (4), 209–227.

Punger, E.M., West, J.J., 2013. The effect of grid resolution on estimates of the burden of ozone and fine particulate matter on premature mortality in the USA. Air Quality, Atmosphere & Health 6, 563–573.

Pye, H., Chan, A., Barkley, M., Seinfeld, J., 2010. Global modeling of organic aerosol: the importance of reactive nitrogen (NO x and NO 3). Atmos. Chem. Phys. 10 (22), 11261–11276. https://doi.org/10.5194/acp-10-11261-2010.

Sacks, W.J., Deryng, D., Foley, J.A., Ramankutty, N., 2010. Crop planting dates: an analysis of global patterns. Global Ecol. Biogeogr. 19 (5), 607–620. https://doi.org/10.1111/j.1466-8238.2010.00551.x.

Schneidemesser, E., Monks, P.S., Allan, J.D., Bruhwiler, L., Forster, P., Fowler, D., Lauer, A., Morgan, W.T., Paasonen, P., Righi, M., 2015. Chemistry and the linkages between air quality and climate change. Chem. Rev. 115 (10), 3856–3897. https://doi.org/10.1021/acs.chemrev.5b00089.

Tai, A.P., Martin, M.V., Heald, C.L., 2014. Threat to future global food security from climate change and ozone air pollution. Nat. Clim. Change 4 (9), 817–821. https://doi.org/10.1038/nclimate2317.

Thurston, G.D., Bell, M.L., 2021. The human health co-benefits of air quality improvements associated with climate change mitigation. In: Climate Change and Global Public Health. Springer, pp. 181–202.

Travis, K.R., Jacob, D.J., Fisher, J.A., Kim, P.S., Marais, E.A., Zhu, L., Yu, K., Miller, C.C., Yantosca, R.M., Sulprizio, M.P., 2016. Why do models overestimate surface ozone in the Southeast United States? Atmos. Chem. Phys. 16 (21), 13561–13577.

U.S. Environmental Protection Agency Clean Air Markets Division. (n.d.). Clean Air Status and Trends Network (CASTNET). Hourly Ozone, Hourly PM2.5. Retrieved April 13, 2022, from www.epa.gov/castnet.

Van Dingenen, R., Dentener, F.J., Raes, F., Krol, M.C., Emberson, L., Cofala, J., 2009. The global impact of ozone on agricultural crop yields under current and future air quality legislation. Atmos. Environ. 43 (3), 604–618. https://doi.org/10.1016/j.atmosenv.2008.10.033.

Vandyck, T., Keramidas, K., Kitous, A., Spadaro, J.V., Van Dingenen, R., Holland, M., Saveyn, B., 2018. Air quality co-benefits for human health and agriculture counterbalance costs to meet Paris Agreement pledges. Nat. Commun. 9 (1), 1–11. https://doi.org/10.1038/s41467-018-06885-9.

Wang, F., Lin, T., Feng, J., Fu, H., Guo, Z., 2015. Source apportionment of polycyclic aromatic hydrocarbons in PM2. 5 using positive matrix factorization modeling in Shanghai, China. Environmental Science: Process. Impacts 17 (1), 197–205.

Wang, Y., Zhang, Y., Hao, J., Luo, M., 2011. Seasonal and spatial variability of surface ozone over China: contributions from background and domestic pollution. Atmos. Chem. Phys. 11 (7), 3511–3525.

Weng, H.-J., Lin, J.-T. *, Martin, R., Millet, D. B., Jaeglé, L., Ridley, D., Keller, C., Li, C., Du, M.-X., and Meng, J., Global high-resolution emissions of soil NOx, sea salt aerosols, and biogenic volatile organic compounds, Scientific Data, 7, 148, doi: 10.1038/s41597-020-0488-5, 2020.

West, J.J., Smith, S.J., Silva, R.A., Naik, V., Zhang, Y., Adelman, Z., Fry, M.M., Anenberg, S., Horowitz, L.W., Lamarque, J.-F., 2013. Co-benefits of mitigating global greenhouse gas emissions for future air quality and human health. Nat. Clim. Change 3 (10), 885–889. https://doi.org/10.1038/nclimate2009.

Xiong, Y., Partha, D., Prime, N., Smith, S.J., Mariscal, N., Salah, H., Huang, Y., 2022. Long-term trends of impacts of global gasoline and diesel emissions on ambient PM2. 5 and O3 pollution and the related health burden for 2000–2015. Environ. Res. Lett. 17 (10), 104042. https://doi.org/10.1088/1748-9326/ac9422.

Ye, Z., Liu, J., Gu, A., Feng, F., Liu, Y., Bi, C., et al., 2017. Chemical characterization of fine particulate matter in Changzhou, China, and source apportionment with offline aerosol mass spectrometry. Atmos. Chem. Phys. 17 (4), 2573–2592.

Zhang, L., Jacob, D.J., Downey, N.V., Wood, D.A., Blewitt, D., Carouge, C.C., van Donkelaar, A., Jones, D.B., Murray, L.T., Wang, Y., 2011. Improved estimate of the policy-relevant background ozone in the United States using the GEOS-Chem global model with 1/2× 2/3 horizontal resolution over North America. Atmos. Environ. 45 (37), 6769–6776. https://doi.org/10.1016/j.atmosenv.2011.07.054.